Heart and Vessels (2019) 34:177–188
https://doi.org/10.1007/s00380-018-1223-4

ORIGINAL ARTICLE

A novel mutation *KCNQ1*p.Thr312del is responsible for long QT syndrome type 1

Xiao-Meng Chen[1] · Kai Guo[1] · Hong Li[2] · Qiu-Fen Lu[1] · Chao Yang[3] · Ying Yu[1] · Jian-Wen Hou[1] · Yu-Dong Fei[1] · Jian Sun[1] · Jun Wang[1] · Yi-Xue Li[2] · Yi-Gang Li[1]

Received: 13 March 2018 / Accepted: 6 July 2018 / Published online: 14 July 2018

Abstract

Patients with high-risk long QT syndrome (LQTS) mutations may experience life-threatening cardiac events. The present study sought to characterize a novel pathogenic mutation, *KCNQ1*p.Thr312del, in a Chinese LQT1 family. Clinical and genetic analyses were performed to identify this novel causative gene mutation in this LQTS family. Autosomal dominant inheritance of *KCNQ1*p.T312del was demonstrated in the three-generation pedigree. All mutation carriers presented with prolonged QT intervals and experienced recurrent syncope during exercise or emotional stress. The functional consequences of the mutant channel were investigated by computer homology modeling as well as whole-cell patch-clamp, western-blot and co-immunoprecipitation techniques using transfected mammalian cells. T312 is in the selectivity filter (SF) of the pore region of the *KCNQ1*-encoded channel. Homology modeling suggested that secondary structure was altered in the mutant SF compared with the wild-type (WT) SF. There were no significant differences in $K_v7.1$ expression, membrane trafficking or physical interactions with *KCNE1*-encoded subunits between the WT and mutant transfected channels. However, the *KCNQ1*p.T312del channels expressed in transfected cells were non-functional in the absence or presence of auxiliary *KCNE1*-subunits. Dominant-negative suppression of current density and decelerated activation kinetics were observed in cells expressing *KCNQ1*WT and *KCNQ1*p.T312del combined with *KCNE1* (*KCNQ1*WT/p.T312del + *KCNE1* channels). Those electrophysiological characteristics underlie the pathogenesis of this novel mutation and also suggest a high risk of cardiac events in patients carrying *KCNQ1*p.T312del. Although protein kinase A-dependent current increase was preserved, a significant suppression of rate-dependent current facilitation was noted in the *KCNQ1*WT/p.T312del + *KCNE1* channels compared to the WT channels during 1- and 2-Hz stimulation, which was consistent with the patients' phenotype being triggered by exercise. Overall, *KCNQ1*p.Thr312del induces a loss of function in channel electrophysiology, and it is a high-risk mutation responsible for LQT1.

Keywords Electrophysiology · Long QT syndrome · *KCNQ1* · Selectivity filter

Electronic supplementary material The online version of this article (https://doi.org/10.1007/s00380-018-1223-4) contains supplementary material, which is available to authorized users.

Xiao-Meng Chen and Kai Guo contributed equally to this work.

✉ Yi-Xue Li
yxli@sibs.ac.cn

✉ Yi-Gang Li
liyigang@xinhuamed.com.cn

[1] Department of Cardiology, School of Medicine, Xinhua Hospital, Shanghai Jiao Tong University, 1665 Kongjiang Road, Shanghai 200092, China

[2] Key Lab of Computational Biology, CAS-MPG Partner Institute for Computational Biology, Shanghai Institutes for Biological Sciences, Chinese Academy of Sciences, Shanghai 200031, China

[3] Xinhua Translational Institute for Cancer Pain, School of Medicine, Xinhua Hospital (Chongming), Shanghai Jiao Tong University, Shanghai 202150, China

Introduction

Congenital long QT syndrome (LQTS) is an inherited channelopathy associated with a prolonged QT interval on electrocardiogram (ECG). It is a leading cause of sudden cardiac death, especially among the young population [1]. LQTS type 1 (LQT1), which is caused by loss-of-function mutations in the *KCNQ1* gene, accounts for approximately 35% of genotype-positive LQTS cases. Variable penetrance has been reported in LQTS. About 37% of LQT1 patients display normal QT intervals at rest and are usually considered to be at low risk for cardiac events [2]. Accordingly, risk stratification is very important for the management of LQTS patients. Recently, genetic and functional parameters, including location and type of mutation and degree of dysfunction have been considered for risk stratification of LQTS patients, in addition to classical clinical parameters, such as age, gender, QTc interval and history of cardiac events [3–5].

KCNQ1 alone encodes the voltage-gated potassium channel $K_v7.1$. When $K_v7.1$ (the α-subunit) co-assembles with the auxiliary β-subunit (encoded by *KCNE1*), the induced current is very similar to the slowly activating delayed rectifier (I_{Ks}) potassium current in cardiac tissue [6]. The I_{Ks} current is an important component of ventricular repolarization reserve, especially in response to sympathetic nerve activation [7, 8]. Therefore, LQT1 patients tend to present with cardiac events during exercise or emotional stress owing to the reduced I_{Ks} current and further prolonged QT intervals under elevated sympathetic tone [9, 10].

The pore region of the potassium channel is enclosed by the pore loops of four α-subunits with a central ion-conducting pathway termed the selectivity filter (SF) [11]. Rapid and exclusive K^+ ion conduction is the physiological function of the SF. The narrowest part of the SF comprises the conserved signature sequence Thr-Ile/Val-Gly-Tyr-Gly (TXGYG), which is found in all potassium channels (Supplement-Fig. 1) [11, 12].

In the present study, we report a new *KCNQ1* mutation, p.Thr312del, which was identified in a Chinese family. Family members carrying this mutation exhibited prolonged corrected-QT (QTc) intervals and recurrent syncope. Functional studies were designed to evaluate the specific characteristics of this new mutation.

Methods

Detailed methods are provided in the Online-Supplement.

Clinical investigation

The pedigree study was based on findings in a family with a 4-year-old index patient suffering from recurrent syncope. Detailed medical histories, physical examinations, ECG, echocardiography, and serum biochemical analyses were conducted for all eight family members. LQTS was diagnosed based on a recently released expert consensus statement [13]. QT intervals were measured in lead II or V5 and corrected for heart rate using Bazett's formula ($QTc = QT/RR^{1/2}$).

Genetic testing

The genetic analysis protocol was approved by the institutional ethics committee and executed in accordance with its guidelines. Written informed consent was obtained from every subject prior to the analysis. Whole-exome sequencing was performed using extracted genomic DNA, and the identified mutation was analyzed and verified twice via independent polymerase chain reaction (PCR) amplification and sequencing.

Mutagenesis and electrophysiological analysis

The mutation in human *KCNQ1* was introduced using PCR-based site-directed mutagenesis. Further analyses were performed with HEK293 and CHO cells at 48–72 h after transfection. Membrane currents were measured with whole-cell patch clamp techniques as previously described [14]. Data were analyzed using pCLAMP 10 (Molecular Devices, CA, USA) and Origin Pro 9.0 (OriginLab Corporation, MA, USA) software.

Western blotting, co-immunoprecipitation and confocal microscopic analyses

Plasmids carrying wild-type (WT) and mutant green fluorescent protein (GFP)-tagged *KCNQ1* were separately transfected into HEK293 cells. Cells were then prepared for western blotting, co-immunoprecipitation and confocal microscopy at 48 h after transfection. Anti-$K_v7.1$ (Alomone Labs, Jerusalem, Israel) and anti-KCNE1 (Santa Cruz, TX, USA) were used as primary antibodies.

Molecular structural model

The homology modeling of *KCNQ1*-encoded $K_v7.1$ was carried out using Discovery Studio 4.0 (Accelrys, CA, USA). The open-state model was based on the template of the potassium channel from *Streptomyces lividans* (KcsA, PDB: 1JQ1), and the close-state model was based on potassium voltage-gated channel subfamily A member 2 (Kv1.2, PDB: 2R9R).

Statistics

Data are presented as the mean ± standard error. Student's *t* test was performed for comparisons between two groups. One-way analysis of variance (ANOVA) with Bonferroni post hoc analysis was performed for multiple-group comparisons. A *P* value less than 0.05 was considered statistically significant.

Results

Case description

This study was conducted in a three-generation Chinese family; the pedigree is depicted in Fig. 1a. Structural heart disease and acquired LQTS were excluded before diagnosis. The index patient (III:1) was a 4-year-old boy exhibiting a prolonged QT interval (QTc = 495 ms) on resting ECG (Fig. 1c). He was first diagnosed with LQTS with syncope during physical activity at 2 years of age, and he has since suffered from recurrent syncope, particularly during exercise. Two other family members (I:2 and II:3) also presented recurrent syncope triggered by exercise or emotional stress and QTc interval prolongation on 12-lead ECG (Fig. 1c). One patient (I:2) received an implantable cardioverter defibrillator due to the frequent occurrence of ventricular fibrillation. ECG results were negative for other family members without syncope or other LQTS-related symptoms. In addition, negative results were obtained through physical examinations, echocardiography and serum biochemical analyses for all family members.

Mutation analysis

All three symptomatic LQTS patients harbored the same non-frame-shift deletion on one chromosome. As illustrated in Fig. 1b, this heterozygous mutation is located in exon 7 of *KCNQ1* and leads to the deletion of one amino acid: threonine 312. Autosomal dominant inheritance of the mutation was observed in the three-generation pedigree (Fig. 1a). Moreover, this novel mutation was observed in only affected family members; members without LQTS did not carry this mutation. No other mutant alleles were identified during sequencing (minor allele frequency < 0.01 in 45 LQTS-related candidate genes). Homology modeling demonstrated that the deleted amino acid T312 is located in the pore loop region of the *KCNQ1*-encoded potassium channel (Fig. 1d). Notably, it is situated at the beginning of the conserved signature sequence of the SF (Supplement-Fig. 1). A prominent difference in secondary structure between the WT and mutant SFs was predicted by homology modeling analysis via the superimposition of the WT and mutant S5–S6 domains (Fig. 1e). This result suggests that a significant difference in electrophysiological characteristics may exist between the WT and mutant channels.

Impact of *KCNQ1*p.T312del on channel trafficking and interaction with *KCNE1*

Some pathogenic *KCNQ1* mutations were reported to cause the trafficking defect that leads to a loss-of-function of K_v7.1 channel [15]. Expression of the *KCNQ1*-encoded protein was evaluated in HEK293 cells expressing either *KCNQ1*WT, *KCNQ1*p.T312del alone or a combination of *KCNQ1*WT and *KCNQ1*p.T312del in a 1:1 mass ratio (*KCNQ1*WT/p.T312del). A clear membrane associated fluorescence was detected in confocal images of all three conditions (Fig. 2a–c). Significant differences in protein expression were not observed among the transfected cells by western blotting ($P = 0.341$, $n = 4$ cell cultures for each condition, Fig. 2d). These results indicate that *KCNQ1*p.T312del has little effect on channel expression and trafficking to the membrane.

In addition, physical interactions between subunits encoded by the *KCNQ1* and *KCNE1* genes were investigated in cells co-expressing *KCNE1* with either *KCNQ1*WT or *KCNQ1*p.T312del. As shown in Fig. 2e, the WT and mutant cell lysates displayed similar protein levels of the *KCNE1*-encoded subunit after immunoprecipitation with an anti-K_v7.1 antibody. The co-immunoprecipitation results suggest that physical binding to the *KCNE1*-encoded subunit was not interrupted by the *KCNQ1*p.T312del mutation.

Electrophysiological characterization of *KCNQ1*p.T312del channels

Further electrophysiological characterization of the effects of *KCNQ1*p.Thr312del was explored by heterologous expression in CHO cells. As shown in the inset of Fig. 3a, the steady-state current was activated by 5-s depolarizing step pulses from −60 to 60 mV, and the tail current was subsequently elicited at −40 mV. A barely detectable potassium current was detected in cells expressing *KCNQ1*p.Thr312del, which was comparable to current detected in untransfected CHO cells (Fig. 3b). Similar results were observed in HEK293 cells expressing homotetrameric *KCNQ1*p.T312del, which yielded virtually no current, in contrast to the endogenous large potassium current in HEK293 cells (Supplement-Fig. 2). Therefore, a non-functional channel is produced by the *KCNQ1*p.Thr312del mutant alone.

As shown in Fig. 3, a dominant-negative effect was observed in CHO cells expressing *KCNQ1*WT/p.T312del, which exhibited prominently reduced current amplitudes and significant inhibition of current–voltage relationships compared with CHO cells expressing *KCNQ1*WT. The

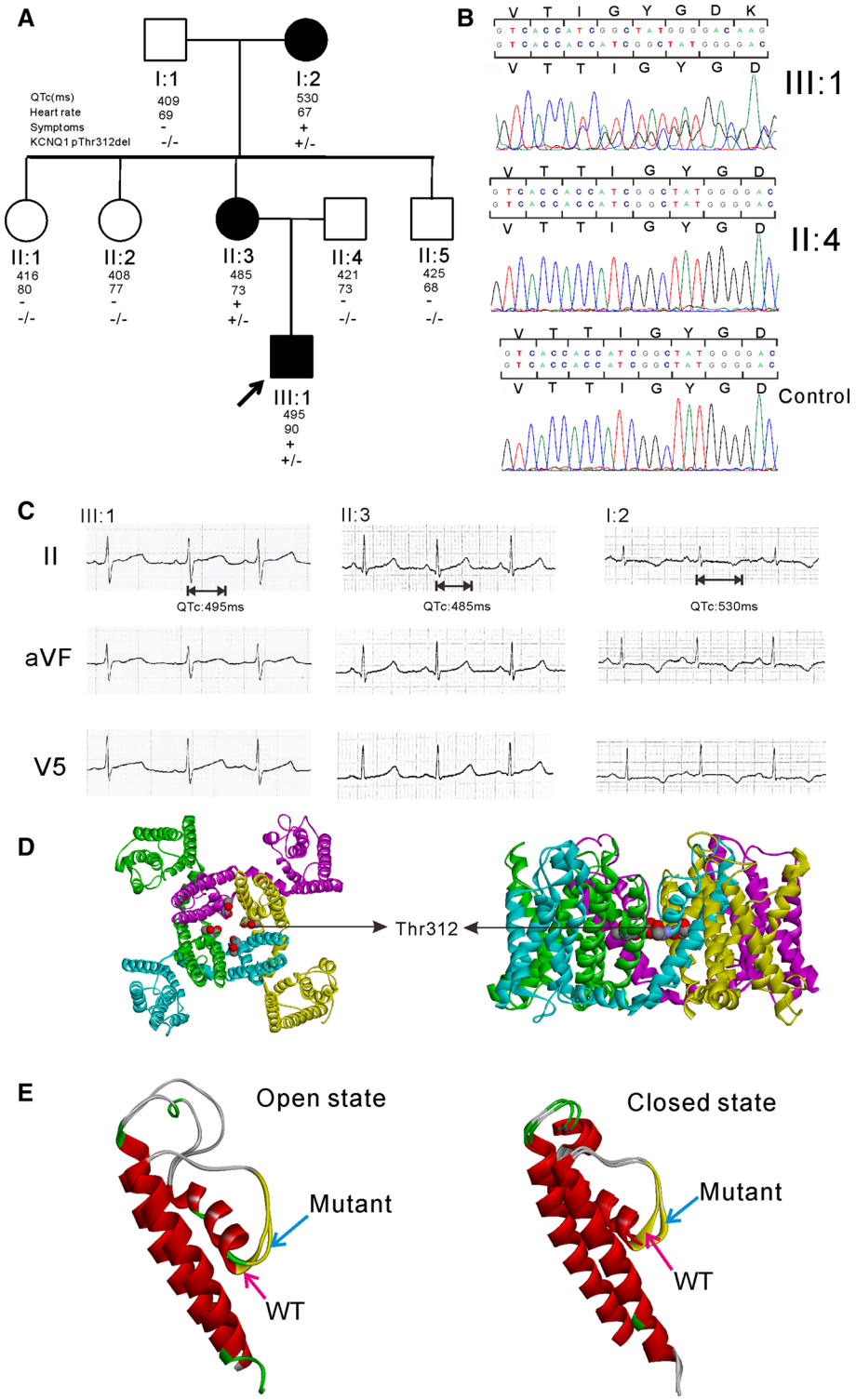

Fig. 1 Pedigree and mutation detection. **a** Family pedigree. Males are denoted by squares, and circles indicate females. Clinically affected individuals are shown as filled symbols, and normal individuals are shown as empty symbols. The index patient is indicated by an arrow. **b** Comparison of the screened sequences of III:1 and II:4 with a normal control population (without LQTS). **c** Representative ECG traces in lead II of the affected individuals in this family. **d** Location of the mutated Thr312 in the open-state $K_v7.1$ homology model, top view (left) and side view (right). Each subunit is colored differently. Thr312 is denoted by the black arrow, and the carbon, nitrogen and oxygen atoms of threonine are represented by gray, blue and red balls, respectively, in each subunit. **e** Superimposed WT and mutant S5–S6 domains of a single *KCNQ1*-encoded subunit in the open state (left) and the closed state (right), which are colored based on the secondary structure. In addition, the structure of the SF is highlighted in yellow. The WT SF is marked by the magente arrow, and the mutant SF is marked by the blue arrow

steady-state current amplitude at 60 mV in *KCNQ1*WT/p.Thr312del-expressing cells was reduced by approximately 83.1% of that in cells expressing *KCNQ1*WT and approximately 87.0% of that at 30 mV (Fig. 3c, $P < 0.05$ vs. *KCNQ1*WT, $n = 8–7$, 60 mV: 23.738 ± 6.217 vs. 140.604 ± 23.002, pA/pF, 30 mV: 13.151 ± 3.512 vs. 101.125 ± 15.503, pA/pF). A 91.3% reduction in the peak tail current, which was elicited at −40 mV after depolarizing to 30 mV, was observed in *KCNQ1*WT/p.Thr312del-expressing cells compared with *KCNQ1*WT-expressing cells (Fig. 3d, $P < 0.05$ vs. *KCNQ1*WT, $n = 8–7$, 2.608 ± 0.720 vs. 29.837 ± 5.378, pA/pF).

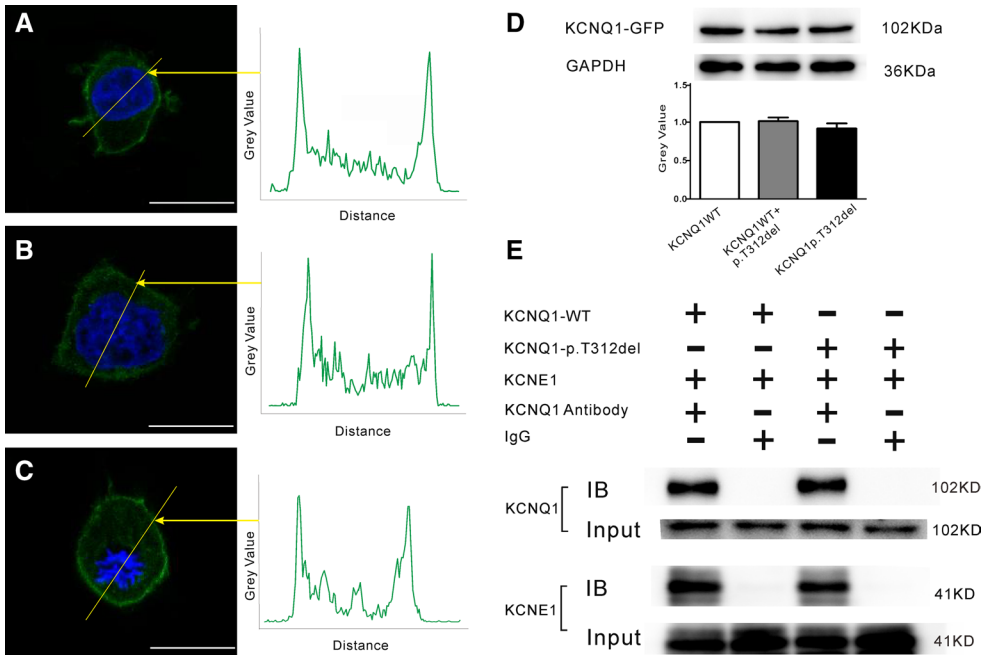

Fig. 2 *KCNQ1* protein expression and interaction with *KCNE1*-encoded subunit in transfected HEK293 cells. **a–c** Confocal images of GFP-*KCNQ1*-encoded protein expression: cells expressing *KCNQ1*WT (**a**), *KCNQ1*WT/p.T312del (**b**), and *KCNQ1*p.T312del (**c**) plasmids. Relative signal intensity was measured based on the cross-section of the labeled yellow line. Calibration bars are 20 µm. Intense membrane-associated signals are displayed under the three transfection conditions. **d** Western blotting images of the *KCNQ1*-encoded protein. The relative level of *KCNQ1* protein expression normalized to GAPDH is indicated by the bar graph ($P=0.341$, $n=4$ for all conditions). **e** Co-immunoprecipitation results for the *KCNE1*-encoded protein in lysates of transfected cells. Lysates of cells expressing *KCNQ1*WT + *KCNE1* and *KCNQ1*p.T312del + *KCNE1* were separately immunoprecipitated with an anti-K_v7.1 antibody or control rabbit IgG and then immunoblotted with an anti-KCNE1 or anti-K_v7.1 antibody. *IB* immunoblotting

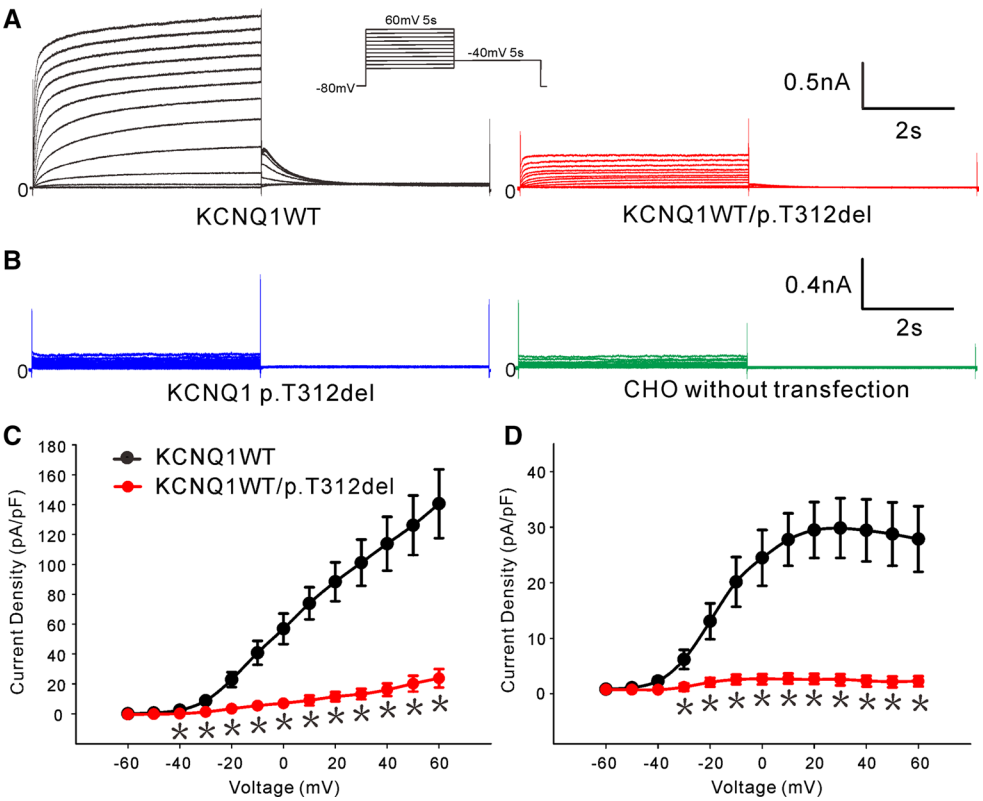

Fig. 3 Properties of *KCNQ1*WT and *KCNQ1*p.T312del currents in CHO cells. **a** Representative current traces from CHO cells expressing *KCNQ1*WT (black) and *KCNQ1*WT/p.T312del (red). **b** Current traces in *KCNQ1*p.T312del-transfected CHO cells (blue) and untransfected cells (green). **c** Comparison of the steady-state current–voltage relationship between *KCNQ1*WT ($n=7$) and *KCNQ1*WT/p.T312del ($n=8$) currents, as determined at the end of the depolarizing pulses. **d** Peak tail current–voltage relationship in *KCNQ1*WT- ($n=7$) and *KCNQ1*WT/p.T312del- ($n=8$) transfected CHO cells. *$P<0.05$, vs. *KCNQ1*WT

Properties of *KCNQ1*p.T312del in the presence of *KCNE1*

When the $K_v7.1$ co-assembles with the *KCNE1* subunit, the induced current closely resembles the I_{Ks} current, with characteristics of slow activation and deactivation as well as non-inactivation [16]. A typical slowly activating large outward current was produced by 5-s depolarizing pulses in CHO cells co-transfected with *KCNQ1*WT and *KCNE1* (*KCNQ1*WT + *KCNE1*, Fig. 4a, protocol in the inset).

Identical to the recording of *KCNQ1*p.T312del channels, *KCNQ1*p.T312del did not yield functional currents in the presence of *KCNE1* in either CHO or HEK293 cells (Fig. 4b and Supplement-Fig. 3). Accordingly, electrophysiological characteristics were compared between cells expressing *KCNQ1*WT and *KCNQ1*WT/p.Thr312del in combination with *KCNE1* (*KCNQ1*WT + *KCNE1* channels vs. *KCNQ1*WT/p.T312del + *KCNE1* channels).

A significant dominant-negative effect was generated by the mutant subunit found in both cell lines (CHO cells: Fig. 4, Table 1; HEK293 cells: Supplement-Fig. 4, Supplement-Table 1). In Fig. 4c, e, significant loss of function in the *KCNQ1*p.Thr312del channels was revealed by plotting both the steady-state current and peak tail current as a function of depolarizing potentials. As depicted in Fig. 4d, the steady-state current density measured at the end of a 5-s depolarizing pulse at 30 mV was 245.09 ± 43.78 pA/pF for *KCNQ1*WT + *KCNE1* channels ($n = 6$) and 65.81 ± 14.46 pA/pF for *KCNQ1*WT/p.T312del + *KCNE1* channels ($n = 7$), for an approximate 73.1% reduction ($P = 0.002$). In addition, a more than 50% reduction in the tail current of cells expressing mutant subunits was also noted, especially when elicited at positive depolarizing potentials (Fig. 4d and Table 1, $P < 0.05$ vs. *KCNQ1*WT + *KCNE1* channels, $n = 7$–6). Voltage-dependent steady-state activation was based on the peak tail current, with a positive-shift tendency of approximately 8 mV for the half-maximal activation potential ($V_{1/2}$) in the mutant channels (Fig. 4f and Table 1, $P = 0.069$ vs. *KCNQ1*WT + *KCNE1*, $n = 7$–6). A significant difference in the activation kinetics of *KCNQ1*WT/p.T312del + *KCNE1* channels was also noted (Fig. 4g). The activation time constant (τ_{act}) was assessed by 5-s depolarizing traces from 10 to 60 mV. An increased τ_{act} was observed for *KCNQ1*WT/p.T312del + *KCNE1* channels at a depolarizing potential of 30 mV, reflecting an approximately 1.3-fold slower activation time than *KCNQ1*WT + *KCNE1* channels (Fig. 4g and Table 1, $P = 0.041$ vs. *KCNQ1*WT + *KCNE1*, $n = 10$–7). Regarding the deactivation time constant, a significant difference was not observed between the two channels (Fig. 4h and Table 1, $P > 0.05$ vs. *KCNQ1*WT + *KCNE1*, $n = 11$–6). Similar electrophysiological properties for *KCNQ1*WT/p.T312del+ *KCNE1* channels were confirmed in transfected HEK293 cells (Supplement-Fig. 4).

Effects of *KCNQ1*p.T312del on protein kinase A (PKA) activation and rate dependence

The I_{Ks} current is particularly important for repolarization when β-adrenergic receptors are stimulated and PKA and cytoplasmic cyclic adenosine monophosphate (cAMP) expression levels are further up-regulated [10]. To mimic this effect on mutant I_{Ks} channels, A-kinase anchoring protein (AKAP/Yotiao), an essential component of PKA-mediated I_{Ks} activation, was expressed with *KCNQ1*WT + *KCNE1* or *KCNQ1*WT/p.T312del + *KCNE1* in HEK293 cells. To elevate cytoplasmic cAMP expression, 100 μM 3-isobutyl-1-methylxanthine (IBMX) and 10 μM forskolin were also added to the external solution. After incubation with these drugs, similar increases in the steady-state current recording from 20 to 60 mV were observed in the two channels (Fig. 5a, b, $P > 0.05$, $n = 9$–6).

Furthermore, the I_{Ks} current can rise in response to a fast pacing rate. Therefore, rate-dependent current facilitation under the mutant condition was investigated at 1- and 2-Hz pacing rates. The I_{Ks}-like currents were activated in response to the two pacing rates by a series of 40 continuous pulses from − 80 to 40 mV with a 350-ms pulse duration (inset in Fig. 5c). In addition, the elicited traces before and after drug administration are shown in Supplementary Fig. 5. As described in Fig. 5c, d, the current amplitude measured at the end (350-ms) of each pulse normalized to the maximum activated current amplitude was plotted as a function of the pulse number under both WT and mutant conditions. The rate-dependent current increase observed in *KCNQ1*WT + *KCNE1* channels exhibited much faster kinetics than that observed in *KCNQ1*WT/p.T312del + *KCNE1* channels (Figs. 3d, 5c). To better quantify this increase, we further compared the current amplitude at the end of the 1st and 40th pulses. As shown in Fig. 5e, significant current accumulation after 40 continuous pulses was noted at the fast rate (2-Hz) for *KCNQ1*WT + *KCNE1* channels regardless of IBMX and forskolin administration (*$P < 0.05$ vs. current amplitude at the 1st pulse, $n = 6$, control condition: 1265.767 ± 248.951 vs. 962.757 ± 189.416, pA, drug condition: 2043.660 ± 539.787 vs. 781.555 ± 143.191, pA). However, this significant current accumulation at 2-Hz was not observed for *KCNQ1*WT/p.T312del + *KCNE1* channels, indicating defective rate-dependent current facilitation in this heteromeric mutant channel. In addition, significant drug-induced increases were found for *KCNQ1*WT + *KCNE1* channels after 40 continuous pulses under both 1- and 2-Hz pacing rates, which suggested that PKA activation may enhance the rate-dependent effect on the WT current (Fig. 5e, #$P < 0.05$ vs. current amplitude at the 40th pulse before drug application, 1-Hz: $n = 7$, 1265.767 ± 248.951 vs. 946.045 ± 168.946, pA,

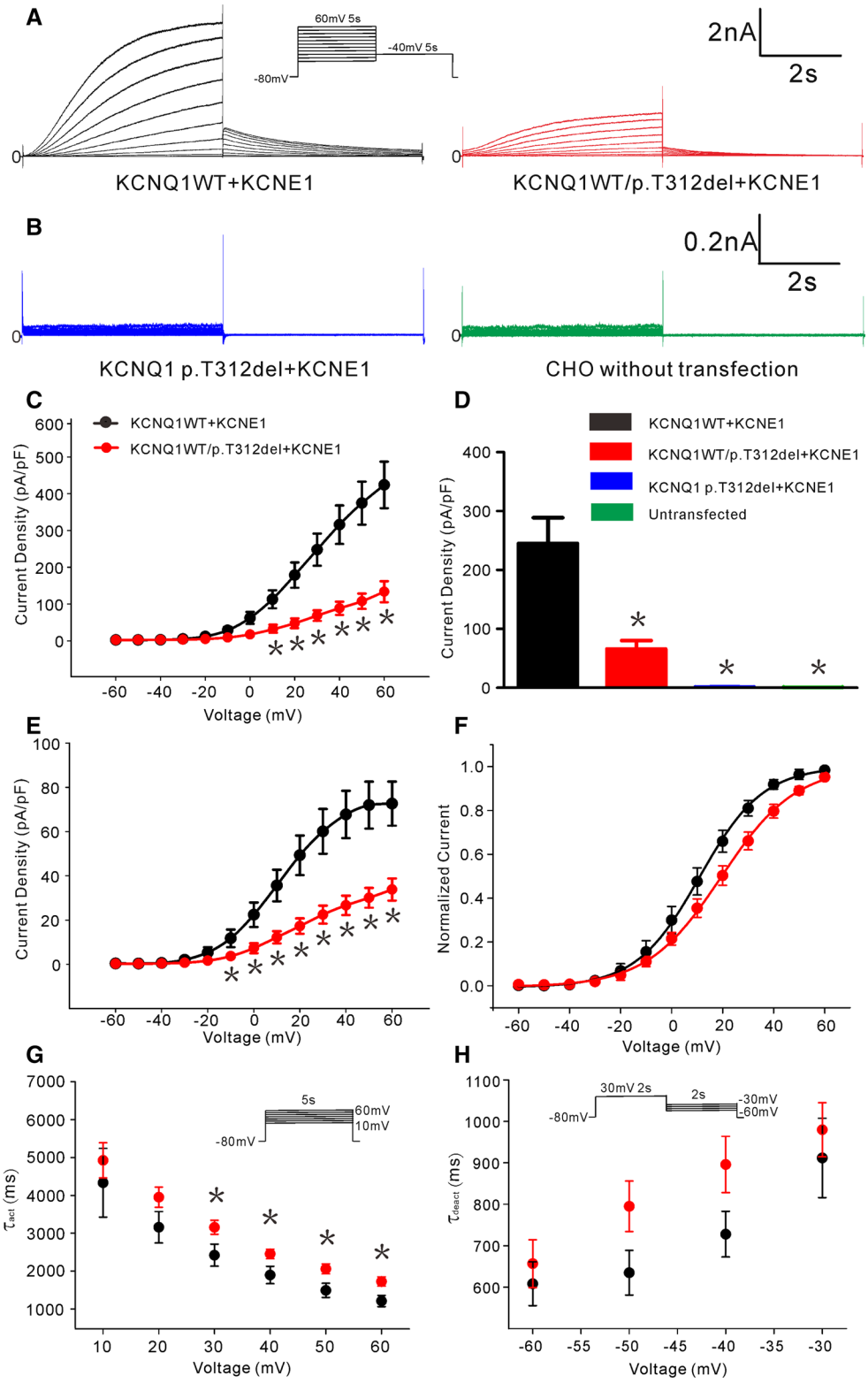

Fig. 4 Electrophysiological characteristics of CHO cells expressing *KCNQ1*WT and *KCNQ1*p.T312del in the presence of *KCNE1*. **a** Representative current traces recorded from CHO cells expressing *KCNQ1*WT + *KCNE1* (black) and *KCNQ1*WT/p.T312del + *KCNE1* (red). **b** Current traces from *KCNQ1*p.T312del + *KCNE1* (blue) and untransfected CHO cells (green). **c** Steady-state current–voltage relationships in *KCNQ1*WT + *KCNE1* ($n = 6$) and *KCNQ1*WT/p.T312del + *KCNE1* cells ($n = 7$). **d** Steady-state current density at a 30-mV depolarized pulse compared among *KCNQ1*WT + *KCNE1* ($n = 6$), *KCNQ1*WT/p.T312del + *KCNE1* ($n = 7$), *KCNQ1*p.T312del + *KCNE1* ($n = 7$) and the untransfected cells ($n = 8$). **e** Peak tail current–voltage relationships among *KCNQ1*WT + *KCNE1* ($n = 6$) and *KCNQ1*WT/p.T312del + *KCNE1* cells ($n = 7$). **f** Steady-state activation curve derived by normalizing the tail current. **g** Activation time constants derived from 10- to 60-mV depolarized currents. **h** Deactivation time constants determined by 2-s pulses from −60 to −30 mV. *$P < 0.05$ vs. *KCNQ1*WT + *KCNE1*

2 Hz: $n = 6$, 2043.660 ± 539.787 vs. 1399.621 ± 309.937, pA). Nevertheless, despite preserved PKA-dependent activation of the mutant current, only moderate current increases were observed for the *KCNQ1*WT/p.T312del + *KCNE1* channels in the presence of IBMX and forskolin after 40 continuous pulses under the two pacing rates.

Table 1 Electrophysiological characterization of transfected *KCNQ1*WT + *KCNE1* and *KCNQ1*WT/p.T312del + *KCNE1* channels

	*KCNQ1*WT + *KCNE1*	*KCNQ1*WT/p.T312del + *KCNE1*
Steady-state current density at + 30 mV (pA/pF)	245.094 ± 43.784	65.808 ± 14.455*
Peak tail current density at + 30 mV (pA/pF)	60.099 ± 10.100	22.438 ± 4.068*
$V_{1/2}$(mV)	11.084 ± 3.424	19.485 ± 2.514
K (mV)	12.439 ± 0.432	14.593 ± 0.744*
Tau activation at 30 mV (ms)	2420.449 ± 292.467	3157.061 ± 185.811*
Tau deactivation at − 40 mV after depolarizing to 30 mV(ms)	727.879 ± 55.059	895.820 ± 67.804

$V_{1/2}$ is the voltage for half-maximal activation and *K* is the slope factor

*$P < 0.05$ vs. *KCNQ1*WT + *KCNE1*. Data are reported as mean ± SEM

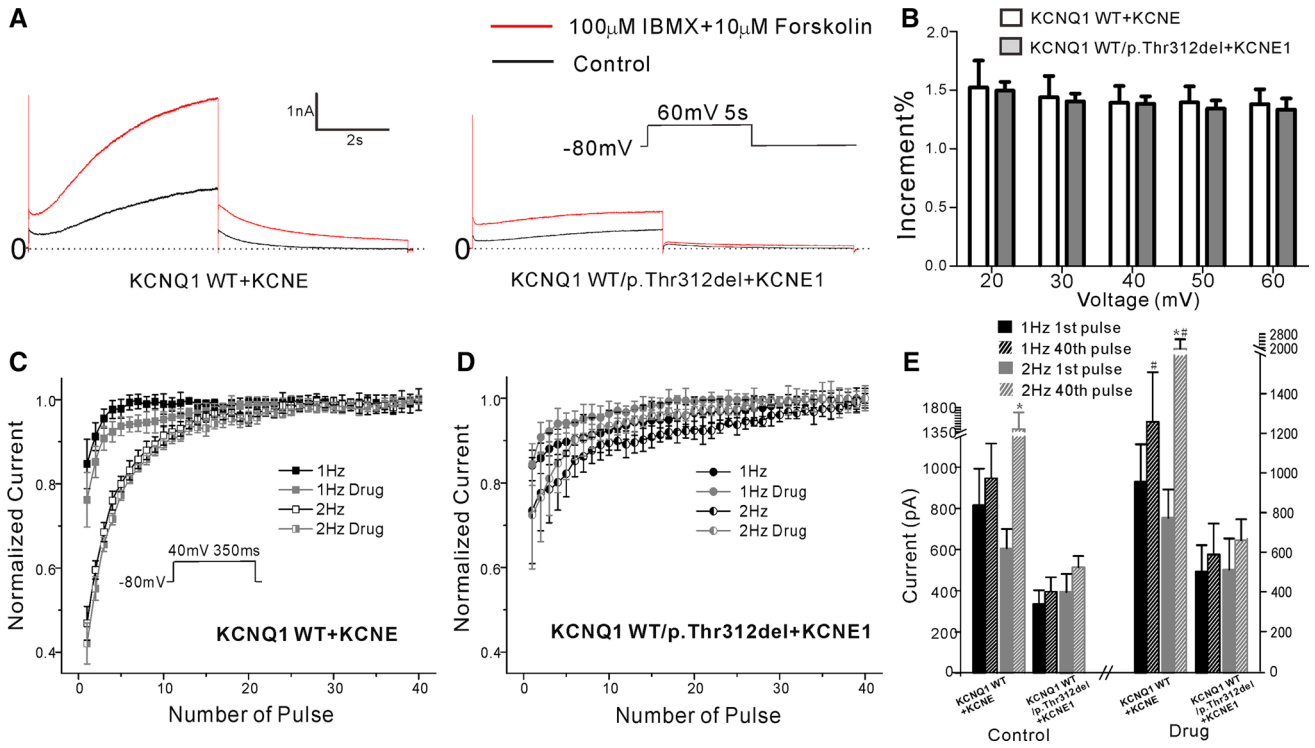

Fig. 5 PKA- and rate-dependent regulation of *KCNQ1*WT + *KCNE1* and *KCNQ1*WT/p.T312del + *KCNE1* channel currents. **a** Current traces recorded from HEK293 cells expressing *KCNQ1*WT + *KCNE1* (left) or *KCNQ1*WT/p.T312del + *KCNE1* (right) before (control) and after drug (IBMX and forskolin) administration. Plasmids encoding Yotiao were also co-transfected into HEK293 cells. **b** Peak current from 20 to 60 mV after drug application relative to that in the control. The current was recorded at the end of the 5-s depolarizing pulses. **c**, **d** Rate-dependent changes in *KCNQ1*WT + *KCNE1* and *KCNQ1*WT/p.T312del + *KCNE1* channels. The current in each pulse was normalized to the maximum current during 40 pulses. **e** Current amplitude measured at the 1st and 40th pulse under 1- and 2-Hz pacing rates in the presence and absence of the drug. *$P < 0.05$ vs. current at the 1st pulse under the 2-Hz pacing rate; #$P < 0.05$ vs. current at the 40th pulse before applying the drug under the same pacing rate

Discussion

The present study identified a novel *KCNQ1* mutation, p.T312del, in the conserved signature sequence of the SF. Typical autosomal dominant inheritance with complete penetrance was evident in our LQT1 pedigree. Homology modeling suggested notable changes in the secondary structure of the mutant SF. Functional studies were performed on transfected mammalian cells to characterize the deleterious effect of this new mutation on channel function.

Dominant-negative effect of *KCNQ1*p.T312del: the underlying pathogenesis

Some LQT1 patients exhibit prolonged QTc intervals in resting ECGs [1, 2]. However, in this LQT1 family, all the *KCNQ1*p.T312del carriers presented with prolonged QTc intervals. As depicted in Table 2, in which we summarize the published SF mutations, most patients with an SF mutation had prolonged QTc intervals at rest and were prone to experiencing cardiac events [15]. Dominant-negative current suppression, which was observed in the functional studies of those reported SF mutations, was considered as the basic pathogenic mechanism [17–19]. In the present study, non-functional channels were confirmed in both CHO and HEK293 cells expressing *KCNQ1*p.T312del (Fig. 3 and Supplement-Fig. 2). In *KCNQ1*WT/p.T312del-expressing cells, a dominant-negative effect was observed, and a greater than 50% reduction was noted in both the steady-state current amplitude and the peak tail current amplitude compared to WT (Fig. 3).

The underlying pathogenesis, dominant-negative current suppression, indicates a significant reduction in K^+ ion conduction [20]. Homology modeling in the present study showed that compared to WT, the T312 deletion results in a different SF secondary structure in both the open and closed states (Fig. 1e). Based on the physiological function of the SF, we speculate that this aberrant structure of the mutant SF may contribute to a reduction in K^+ ion permeation. In addition to the pore structure, the energetic equilibrium of the K^+ ion binding configurations inside the SF may also affect K^+ ion conduction [20, 21]. Our current understanding of K^+ ion channel pore structure is mainly derived from studies on KcsA. X-ray and molecular dynamic simulations have revealed four K^+ ion binding sites (sites 1–4) inside the SF, and two K^+ ions typically reside in the SF in two configurations (sites 1 and 3; and sites 2 and 4) under physiological concentrations [22]. As shown by Morais-Cabral et al., the energetic equilibrium between the two configurations ensures the rapid conduction of K^+ ions through the SF [21]. Site 4 comprises the main-chain carbonyl oxygen atoms and hydroxyl oxygen atoms of threonine in the SF (Thr75 in KcsA; Thr312 in K_v7.1) [20]. The electron density analysis by Zhou et al. demonstrated that mutation of KcsA Thr75 to Cys via removal of the threonine hydroxyl resulted in markedly lower electron occupancy at site 4 and disrupted the energetic equilibrium between the two configurations. Their cellular electrophysiological results also confirmed reduced ion conduction in KcsA T75C [20]. In the *KCNQ1*p.T312del mutant channel, the carbonyl and hydroxyl oxygen atoms of T312 are completely eliminated, which may have a damaging effect on the configurations of K^+ ion distribution in the SF and a deleterious impact on normal conduction.

Impaired rate dependence of current facilitation of *KCNQ1*p.T312del: an additive and important alteration

Exercise, such as swimming, is a major trigger associated with cardiac events in LQT1 patients [13]. As summarized in Table 2, most LQT1 patients carrying SF mutations experienced syncope during β-adrenergic stimulation. Although dominant-negative current reduction can largely explain the pathogenesis of *KCNQ1* mutations in the SF, PKA and/or rate-dependent current changes may provide specific insights into the relationship between genotype and phenotype, which has not been investigated in LQT1 patients with SF mutations (Table 2).

In the present study, PKA-dependent activation resulted in increased current in the WT and heteromeric mutant channels. As shown in Fig. 5b, similar increases in the steady-state current were observed in the two channels after the addition of IBMX and forskolin, which hints that PKA-dependent I_{Ks} activation may be preserved in the *KCNQ1*WT/p.T312del + *KCNE1* channel. And further study concerning PKA-dependent I_{Ks} current changes of SF mutant channel remains to be explored.

Nonetheless, our affected patients all presented with recurrent syncope during emotional or exercise stress. Despite preserved PKA-dependent I_{Ks} activation, rate-dependent current accumulation was significantly blunted in *KCNQ1*WT/p.T312del + *KCNE1* channels at a fast pacing rate (such as 2 Hz), which may account for the sympathetic stress-related symptoms (Fig. 5c–e). Of note, decelerated activation kinetics was observed at positive depolarizing potentials in both CHO and HEK293 cells expressing *KCNQ1*p.T312del subunits (Fig. 4 and Supplementary Fig. 4). Such abnormal activation kinetics may contribute to current suppression in *KCNQ1*WT/p.T312del + *KCNE1* channels during fast-rate stimulation. In addition to the dominant-negative effect, properties such as activation kinetics and rate dependence may provide additional insight into the genotype–phenotype relationships underlying SF mutations.

*KCNQ1*p.T312del predicts increased risk of cardiac events in LQT1 patients

In addition to clinical parameters such as age, gender and QTc interval, genetic and functional parameters including location, type of mutation and degree of dysfunction have recently been considered for risk stratification of LQT1 patients [4, 13, 23]. *KCNQ1* mutations in conserved sequences and transmembrane regions as well as the dominant-negative effect of its electrophysiological properties are independent risk factors of cardiac events [3, 15, 24]. Therefore, *KCNQ1*p.T312del and other SF mutations are

Table 2 Summary of published mutations in selectivity filter

	Mutation discovered from unrelated patients	Mutation screened from LQT1 pedigree	Penetrance	Symptoms	QTc	Dominant-negative effect	Trafficing defect	PKA dependent regulation	Rate dependence
T312I	Yes (a, b)	Yes (c, d)	Complete (c)	NG	QTc > 470 ms (c)	Yes (e, f)	UI	UI	UI
T312del	–	Yes (Present study)	Complete	Syncope during exercise or emotional stress	Proband 1: 495 ms Proband 2: 485 ms Proband 3: 530 ms	Yes	NS	NS	Impaired
I313 K	–	Yes (g, h)	Not complete (h)	Syncope (h)	Proband 1: 629 ms Proband 2: 500 ms Proband 3: 508 ms (h)	Yes (h)	NS (h)	UI	UI
I313 M	–	Yes (i)	NG	NG	NG	–	–	–	–
G314A	–	Yes (g, j)	NG	NG	Proband 1: 610 ms Proband 2: 500 ms (j)	–	–	–	–
G314C	Yes (b)	–	–	NG	NG	–	–	–	–
G314D	Yes (a)	–	–	NG	NG	–	–	–	–
G314R	Yes (a)	–	–	NG	NG	–	–	–	–
G314S	Yes (a, b, k)	Yes (g, j, l–p)	Complete (l, m); Not complete (n)	Syncope with specific trigger (k); No SCD, syncope during physical stress (l); SCD and syncope (p)	Proband 1: 622 ms (j); 500 ms (k); Proband 1:450 ms Proband 2:420 ms Proband 3:500 ms (n); 492 ± 26 ms ($n = 7$) (p)	Yes (f, q, r)	UI	UI	UI
Y315C	Yes (a, b)	Yes (d, m, p, s, t)	Complete (m);33% (s); not complete (t)	No SCD (s); Drug induced cardiac arrest (t)	484 ± 38 ms ($n = 13$) (p); QTc > 520 ms (drug-induced) (t)	Yes (t, u)	NS (u)	UI	UI
Y315S	–	Yes (d, l)	Complete (l)	No SCD, syncope during physical stress (l)	NG	Yes (q, r)	UI	UI	UI
G316E	Yes (k, v)	–	–	NG	NG	–	–	–	–
G316R	Yes (a)	–	–	NG	NG	–	–	–	–
G316 V	Yes (b)	–	–	NG	NG	–	–	–	–
D317 N	–	Yes (w, x)	67% (x)	SCD, Syncope during exercise or emotional stress (x)	484 ± 38 ms ($n = 30$) (x)	Yes (w, y)	Yes (y)	UI	UI
D317G	–	Yes (d)	NG	NG	NG	–	–	–	–

NG not given, data is not given in the published papers, *UI* un-investigation, the relevant functional study was not performed in the published studies, – we did not find any relevant published studies, *NS* not significant, the different between the WT and mutant is not significant, *SCD* sudden cardiac death. References (a–y) in Table 2 are listed in Online-Supplement

strongly suggested to be associated with increased risk of cardiac events.

Jons et al. recently demonstrated that LQT1 causative mutations with decelerated activation ($\tau_{act\text{-}mutant}/\tau_{act\text{-}WT} > 1.2$), such as T312I and G314S, independently contribute to cardiac risk [25]. In agreement, $\tau_{act\text{-}mutant}/\tau_{act\text{-}WT}$ in CHO cells expressing *KCNQ1*p.T312del was calculated to be approximately 1.3 at a depolarized potential of 30 mV.

Consistent with the genetic and functional parameters, the 4-year-old index patient in the present pedigree had a prolonged QTc interval (495 ms), experienced his first syncope at 2 years old and displayed recurrence of syncope while on β-blocker therapy. Despite the limited data, most LQT1 patients carrying SF mutations reported experiencing cardiac events (Table 2). LQTS is a classic inherited arrhythmic disease. Recent studies have focused on the relationships between genotype and phenotype in LQTS cases. Genetic and functional parameters of LQTS causative mutations can affect clinical presentation, ECG parameters and prognosis, such as risk stratification or triggers of the cardiac events, especially for LQT1 or LQT2 patients [9, 26]. Our findings from this LQT1 family emphasize the importance of genetic and functional parameters in risk stratification of LQT1 patients.

Study limitations

We did not design a computational model for this mutation to assess changes in action potential. However, our electrophysiological study demonstrated an apparent decrease in mutant I_{Ks} current. Moreover, patients carrying this conserved amino acid mutation presented with prolonged QTc intervals, indirectly illustrating the increase in action potential duration caused by this mutation. Although we did not obtain patient-specific induced pluripotent stem cell-derived cardiomyocytes, functional studies performed with HEK293 and CHO cells provided consistent results and revealed detailed characteristics of this mutation.

Conclusions

The present study discovered the first *KCNQ1* deletion mutation of the signature sequence in the SF. This mutation displayed autosomal dominant inheritance and complete penetrance in the evaluated Chinese LQT1 family. Homology modeling indicated strongly altered secondary structure of the SF due to this novel mutation. Dominant-negative current inhibition was observed in *KCNQ1*p.T312del-expressing mammalian cells. Moreover, the decelerated activation and significant suppression in rate-dependent current facilitation observed in the *KCNQ1*p.T312del mutant channel provided additional insight into its pathogenesis. Clinical parameters as well as genetic and functional parameters illustrate the high risk of cardiac events associated with this mutation.

Funding This work was supported by National Natural Science Foundation of China (no. 81270258), the State Key Program of National Natural Science Foundation of China (no. 81530015), Shanghai City Committee of Science and Technology Research Projects (nos. 12411951900, 13140903801, and 14441902502) and Doctoral Innovation Fund Projects from Shanghai Jiao Tong University School of Medicine (BXJ201427).

Compliance with ethical standards

Conflict of interest The authors declare that they have no conflict of interest.

References

1. Schwartz PJ, Crotti L, Insolia R (2012) Long-QT syndrome: from genetics to management. Circ Arrhythm Electrophysiol 5:868–877
2. Obeyesekere MN, Antzelevitch C, Krahn AD (2015) Management of ventricular arrhythmias in suspected channelopathies. Circ Arrhythm Electrophysiol 8:221–231
3. Jons C, Moss AJ, Lopes CM, McNitt S, Zareba W, Goldenberg I, Qi M, Wilde AA, Shimizu W, Kanters JK, Towbin JA, Ackerman MJ, Robinson JL (2009) Mutations in conserved amino acids in the KCNQ1 channel and risk of cardiac events in type-1 long-QT syndrome. J Cardiovasc Electrophysiol 20:859–865
4. Goldenberg I, Horr S, Moss AJ, Lopes CM, Barsheshet A, McNitt S, Zareba W, Andrews ML, Robinson JL, Locati EH, Ackerman MJ, Benhorin J, Kaufman ES, Napolitano C, Platonov PG, Priori SG, Qi M, Schwartz PJ, Shimizu W, Towbin JA, Vincent GM, Wilde AA, Zhang L (2011) Risk for life-threatening cardiac events in patients with genotype-confirmed long-QT syndrome and normal-range corrected QT intervals. J Am Coll Cardiol 57:51–59
5. Ruwald MH, Xu Parks X, Moss AJ, Zareba W, Baman J, McNitt S, Kanters JK, Shimizu W, Wilde AA, Jons C, Lopes CM (2016) Stop-codon and C-terminal nonsense mutations are associated with a lower risk of cardiac events in patients with long QT syndrome type 1. Heart Rhythm 13:122–131
6. Sanguinetti MC, Curran ME, Zou A, Shen J, Spector PS, Atkinson DL, Keating MT (1996) Coassembly of K(V)LQT1 and minK (IsK) proteins to form cardiac I(Ks) potassium channel. Nature 384:80–83
7. Burashnikov A, Antzelevitch C (2000) Block of IKs does not induce early afterdepolarization activity but promotes β-adrenergic agonist-induced delayed afterdepolarization activity. J Cardiovasc Electrophysiol 11:458–465
8. Heijman J, Spatjens RL, Seyen SR, Lentink V, Kuijpers HJ, Boulet IR, de Windt LJ, David M, Volders PG (2012) Dominant-negative control of cAMP-dependent IKs upregulation in human long-QT syndrome type 1. Circ Res 110:211–219
9. Schwartz PJ, Priori SG, Spazzolini C, Moss AJ, Vincent GM, Napolitano C, Denjoy I, Guicheney P, Breithardt G, Keating MT, Towbin JA, Beggs AH, Brink P, Wilde AA, Toivonen L, Zareba W, Robinson JL, Timothy KW, Corfield V, Wattanasirichaigoon D, Corbett C, Haverkamp W, Schulze-Bahr E, Lehmann MH, Schwartz K, Coumel P, Bloise R (2001) Genotype-phenotype correlation in the long-QT syndrome: gene-specific triggers for life-threatening arrhythmias. Circulation 103:89–95

10. Wu J, Naiki N, Ding WG, Ohno S, Kato K, Zang WJ, Delisle BP, Matsuura H, Horie M (2014) A molecular mechanism for adrenergic-induced long QT syndrome. J Am Coll Cardiol 63:819–827
11. Bernèche S, Roux B (2005) A gate in the selectivity filter of potassium channels. Structure 13:591–600
12. Bichet D, Grabe M, Jan YN, Jan LY (2006) Electrostatic interactions in the channel cavity as an important determinant of potassium channel selectivity. Proc Natl Acad Sci USA 103:14355–14360
13. Priori SG, Blomstrom-Lundqvist C, Mazzanti A, Blom N, Borggrefe M, Camm J, Elliott PM, Fitzsimons D, Hatala R, Hindricks G, Kirchhof P, Kjeldsen K, Kuck KH, Hernandez-Madrid A, Nikolaou N, Norekval TM, Spaulding C, Van Veldhuisen DJ (2015) 2015 ESC Guidelines for the management of patients with ventricular arrhythmias and the prevention of sudden cardiac death: The Task Force for the Management of Patients with Ventricular Arrhythmias and the Prevention of Sudden Cardiac Death of the European Society of Cardiology (ESC)Endorsed by: Association for European Paediatric and Congenital Cardiology (AEPC). Europace 17:1601–1687
14. Chen X, Yu L, Shi S, Jiang H, Huang C, Desai M, Li Y, Barajas-Martinez H, Hu D (2016) Neuronal Nav1.8 channels as a novel therapeutic target of acute atrial fibrillation prevention. J Am Heart Assoc 5:e004050
15. Moss AJ, Shimizu W, Wilde AA, Towbin JA, Zareba W, Robinson JL, Qi M, Vincent GM, Ackerman MJ, Kaufman ES, Hofman N, Seth R, Kamakura S, Miyamoto Y, Goldenberg I, Andrews ML, McNitt S (2007) Clinical aspects of type-1 long-QT syndrome by location, coding type, and biophysical function of mutations involving the KCNQ1 gene. Circulation 115:2481–2489
16. Ruscic KJ, Miceli F, Villalba-Galea CA, Dai H, Mishina Y, Bezanilla F, Goldstein SA (2013) IKs channels open slowly because KCNE1 accessory subunits slow the movement of S4 voltage sensors in KCNQ1 pore-forming subunits. Proc Natl Acad Sci USA 110:E559–E566
17. Ikrar T, Hanawa H, Watanabe H, Okada S, Aizawa Y, Ramadan MM, Komura S, Yamashita F, Chinushi M, Aizawa Y (2008) A double-point mutation in the selectivity filter site of the KCNQ1 potassium channel results in a severe phenotype, LQT1, of long QT syndrome. J Cardiovasc Electrophysiol 19:541–549
18. Kobori A, Sarai N, Shimizu W, Nakamura Y, Murakami Y, Makiyama T, Ohno S, Takenaka K, Ninomiya T, Fujiwara Y, Matsuoka S, Takano M, Noma A, Kita T, Horie M (2004) Additional gene variants reduce effectiveness of beta-blockers in the LQT1 form of long QT syndrome. J Cardiovasc Electrophysiol 15:190–199
19. Ikrar T, Hanawa H, Watanabe H, Aizawa Y, Ramadan MM, Chinushi M, Horie M, Aizawa Y (2009) Evaluation of channel function after alteration of amino acid residues at the pore center of KCNQ1 channel. Biochem Biophys Res Commun 378:589–594
20. Zhou M, MacKinnon R (2004) A mutant KcsA K(+) channel with altered conduction properties and selectivity filter ion distribution. J Mol Biol 338:839–846
21. Morais-Cabral JH, Zhou Y, MacKinnon R (2001) Energetic optimization of ion conduction rate by the K + selectivity filter. Nature 414:37–42
22. Treptow W, Tarek M (2006) K + conduction in the selectivity filter of potassium channels is monitored by the charge distribution along their sequence. Biophys J 91:L81–L83
23. Goldenberg I, Moss AJ, Peterson DR, McNitt S, Zareba W, Andrews ML, Robinson JL, Locati EH, Ackerman MJ, Benhorin J, Kaufman ES, Napolitano C, Priori SG, Qi M, Schwartz PJ, Towbin JA, Vincent GM, Zhang L (2008) Risk factors for aborted cardiac arrest and sudden cardiac death in children with the congenital long-QT syndrome. Circulation 117:2184–2191
24. Shimizu W, Horie M, Ohno S, Takenaka K, Yamaguchi M, Shimizu M, Washizuka T, Aizawa Y, Nakamura K, Ohe T, Aiba T, Miyamoto Y, Yoshimasa Y, Towbin JA, Priori SG, Kamakura S (2004) Mutation site-specific differences in arrhythmic risk and sensitivity to sympathetic stimulation in the LQT1 form of congenital long QT syndrome: multicenter study in Japan. J Am Coll Cardiol 44:117–125
25. Jons C, Jin OU, Moss AJ, Reumann M, Rice JJ, Goldenberg I, Zareba W, Wilde AA, Shimizu W, Kanters JK, McNitt S, Hofman N, Robinson JL, Lopes CM (2011) Use of mutant-specific ion channel characteristics for risk stratification of long QT syndrome patients. Sci Transl Med 3:76ra28
26. Nakano Y, Shimizu W (2016) Genetics of long-QT syndrome. J Hum Genet 61:51–55